Chapter 11

MIMO HSDPA Throughput Measurement Results

Christian Mehlführer, Sebastian Caban, and Markus Rupp

Contents

11.1 Introduction

In this chapter, physical layer throughput measurement results of multiple-input, multiple-output (MIMO) High-Speed Downlink Packet Access (HSDPA) [1] are presented. The results were obtained in two extensive measurement campaigns: The first campaign was carried out in an alpine valley in Austria. Here, the propagation channel had a very small mean root mean square (RMS) delay spread[1] of about one chip (260 ns) due to the fact that scattering objects existed only in the immediate vicinity of the receiver. The second campaign was carried out in the inner city of Vienna, Austria. Here, the propagation conditions were non-line-of-sight with a rather large mean RMS delay spread of about 3.8 chips (1 μs).

In the measurements we considered fast link adaptation [2] and fast hybrid automated repeat request [3], two of the key features of the HSDPA physical layer. We restricted ourselves to the single-user case due to the hardware effort required for multi-user measurements. Another reason for choosing only the single-user case for the measurements is that multi-user scheduling for HSDPA is still a topic in research [4–6]. We furthermore restricted our investigations to slow fading; that is, the channel was assumed constant during the transmission of several sub-frames. This restriction is required by our measurement procedure explained in detail in the section entitled "Measurement Setup and Procedure."

11.2 MIMO HSDPA

In this section, a mathematical description of the (MIMO) HSDPA physical layer is introduced. This description is then used to derive the equalizer at the receiver and to describe the precoding at the transmitter. Furthermore, a throughput-maximizing feedback calculation method is explained.

11.2.1 System Model

Assume the transmission of N_s independently coded and modulated data chip streams, each of length $L_c = L_b + L_f - 1$ chips; L_b and L_f correspond to the channel and the equalizer length, respectively. A block diagram of such a transmission system is shown in Figure 11.1. We define the stacked transmit chip vector $\mathbf{s}_k$ of length $N_s L_c$ at time instant k as:

$$\mathbf{s}_k = \left[\mathbf{s}_k^{(1)T}, \ldots, \mathbf{s}_k^{(N_s)T}\right]^T \tag{11.1}$$

[1] The mean RMS delay spread was calculated by averaging the RMS delay spreads of all channel impulse responses measured in a specific scenario.

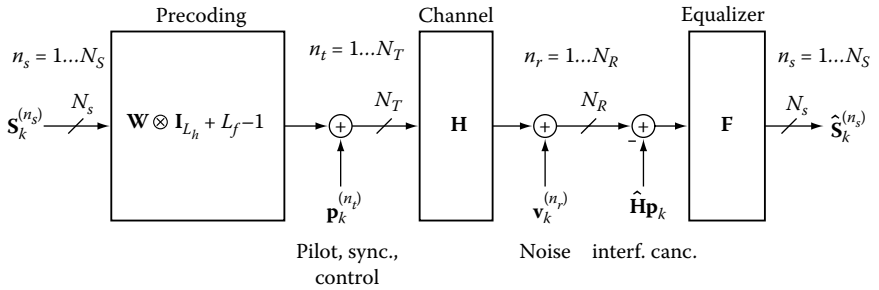

Figure 11.1 Generalized system model of the HSDPA physical layer.

The N_s chip streams are weighted by the $N_T \times N_s$ dimensional precoding matrix

$$\mathbf{W} = \begin{bmatrix} w^{(1,1)} & \dots & w^{(1,N_s)} \\ \vdots & \ddots & \vdots \\ w^{(N_T,1)} & \dots & w^{(N_T,N_s)} \end{bmatrix} \tag{11.2}$$

forming the data chip streams of the N_T transmit antennas. At each transmit antenna, pilot, synchronization, and control channels accumulated in

$$\mathbf{p}_k = \left[\mathbf{p}_k^{(1)T}, \dots, \mathbf{p}_k^{(N_T)T}\right]^T \tag{11.3}$$

are added. Using the $L_c \times L_c$ dimensional identity matrix $\mathbf{I}_{L_c}$, the transmit signal vector $\mathbf{a}_k$ of length $N_T L_c$ at time instant k is given by:

$$\mathbf{a}_k = (\mathbf{W} \otimes \mathbf{I}_{L_c})\mathbf{s}_k + \mathbf{p}_k \tag{11.4}$$

The frequency-selective link between the n_t-th transmit and the n_r-th receive antenna is modeled by the $L_f \times L_c$ dimensional band matrix:

$$\mathbf{H}^{(n_r,n_t)} = \begin{bmatrix} h_0^{(n_r,n_t)} & \dots & h_{L_b-1}^{(n_r,n_t)} & 0 \\ \ddots & & \ddots & \\ 0 & h_0^{(n_r,n_t)} & \dots & h_{L_b-1}^{(n_r,n_t)} \end{bmatrix}; \quad \begin{matrix} 1 \le n_r \le N_R \\ 1 \le n_t \le N_T \end{matrix} \tag{11.5}$$

where the $h_i^{(n_r,n_t)}$ $(i = 0, \dots, L_b - 1)$ represent the channel impulse response between the n_t-th transmit and the n_r-th receive antenna. The entire

frequency-selective MIMO channel is modeled by a block matrix $\mathbf{H}$ consisting of $N_R \times N_T$ band matrices defined in Equation (11.5):

$$\mathbf{H} = \begin{bmatrix} \mathbf{H}^{(1,1)} & \dots & \mathbf{H}^{(1,N_T)} \\ \vdots & \ddots & \vdots \\ \mathbf{H}^{(N_R,1)} & \dots & \mathbf{H}^{(N_R,N_T)} \end{bmatrix} \tag{11.6}$$

At the receiver, additive noise, denoted by $\mathbf{v}_k$, deteriorates the desired signal:

$$\mathbf{b}_k = \mathbf{H}\mathbf{a}_k + \mathbf{v}_k = \mathbf{H}(\mathbf{W} \otimes \mathbf{I}_{L_c})\mathbf{s}_k + \mathbf{H}\mathbf{p}_k + \mathbf{v}_k \tag{11.7}$$

The signal $\mathbf{b}_k$ is then processed in an equalizer $\mathbf{F}$ to obtain an estimate of the transmitted chip stream:

$$\hat{\mathbf{s}}_k = \left[\hat{s}_{k-\tau}^{(1)}, \dots, \hat{s}_{k-\tau}^{(N_s)}\right]^T = \mathbf{F}\mathbf{b}_k = \mathbf{F}\mathbf{H}(\mathbf{W} \otimes \mathbf{I}_{L_c})\mathbf{s}_k + \mathbf{F}\mathbf{H}\mathbf{p}_k + \mathbf{F}\mathbf{v}_k \tag{11.8}$$

The equalizer matrix $\mathbf{F}$ defined by

$$\mathbf{F} = \left[\mathbf{f}^{(1)}, \dots, \mathbf{f}^{(N_s)}\right]^T \tag{11.9}$$

consists of N_s vectors, each having a length of $N_R L_f$. The equalizer and the further processing of the chip stream $\hat{\mathbf{s}}_k$ are explained in the next section.

11.2.2 Receiver

At the receiver, we first perform synchronization and iterative channel estimation according to [7]. After that, the interference of the deterministic signals, that is, the pilot and synchronization channels, is cancelled. Therefore, in Equation (11.8) the term $\mathbf{F}\mathbf{H}\mathbf{p}_k$ is reduced by $\mathbf{F}\hat{\mathbf{H}}\mathbf{p}_k$ and only interference caused by the channel estimation error $(\mathbf{H} - \hat{\mathbf{H}})$ and the data channels remains [8]. Without this interference cancellation, the post equalization signal to interference and noise ratio (SINR) would saturate at about 20 dB. Channel quality indicator (CQI) values requiring higher SINR can thus not be selected, leading to a saturation of the throughput [9–11]. Alternatively to interference cancellation, interference-aware equalization is possible and has been shown to achieve high performance [12,13].

The equalizer coefficients calculated in the Linear Minimum Mean Square Error (LMMSE) sense can be shown [14–16] to be equal to

$$\mathbf{f}^{(n_s)} = \left(\mathbf{H}\left(\mathbf{W}\mathbf{W}^H \otimes \mathbf{I}_{L_c}\right)\mathbf{H}^H + \sigma_v^2 \mathbf{I}_{N_R L_c}\right)^{-1} \cdot \mathbf{H}(\mathbf{W} \otimes \mathbf{I}_{L_c})\mathbf{e}_{\tau+(n_s-1)L_c} \tag{11.10}$$

for the n_s-th data stream. The vector $\mathbf{e}_k$ denotes a unit vector with a single "1" at cursor position k and "0" at all other positions. The calculation of

the equalizer coefficients can be implemented efficiently using Fast Fourier Transform (FFT)-based algorithms as in [17,18], or the conjugated gradient algorithm [19]. This receiver therefore represents a low-complexity HSDPA receiver that is feasible for real-time implementation in a chip [20]. The output of the equalizer $\hat{\mathbf{s}}_k$ is descrambled, despread, soft-demapped, and soft-decoded in a Turbo decoder using eight iterations to obtain the data bits. For the sake of completeness, we note that more complex MIMO receivers (e.g., the LMMSE-Maximum A-Posteriori (MAP)) are known to show only about 1 dB better performance [21] than the standard LMMSE equalizer.

11.2.3 Quantized Precoding

The precoding matrix defined in Equation (11.2) is strongly quantized and chosen from a predefined codebook in HSDPA systems [1]. For single antenna transmissions in which obviously no spatial precoding can be performed, the precoding matrix $\mathbf{W}$ is reduced to a scalar equal to "1":

$$\mathbf{W}^{(\mathrm{SISO})} = 1 \tag{11.11}$$

For multiple antenna transmissions, the precoding matrices are composed of the scalars

$$w_0 = \frac{1}{\sqrt{2}} \tag{11.12}$$

and

$$w_1, w_2 \in \left\{ \frac{1+j}{2}, \frac{1-j}{2}, \frac{-1+j}{2}, \frac{-1-j}{2} \right\}. \tag{11.13}$$

The Transmit Antenna Array (TxAA) transmission mode utilizes two antennas to transmit a single stream. In this mode, the precoding matrix is defined as:

$$\mathbf{W}^{(\mathrm{TxAA})} = \begin{bmatrix} w_0 \\ w_1 \end{bmatrix} \tag{11.14}$$

This means that the signal at the first antenna is always weighted by the same scalar constant w_0, whereas the signal at the second antenna is weighted by w_1, which is chosen in order to maximize the received post equalization SINR [8]. In TxAA, the number of possible precoding matrices is equal to four, corresponding to an amount of 2 bit feedback.

In the case of Double Transmit Antenna Array (D-TxAA) transmission, the precoding matrix is given by:

$$\mathbf{W}^{(\mathrm{D\text{-}TxAA})} = \begin{bmatrix} w_0 & w_0 \\ w_1 & -w_1 \end{bmatrix} \tag{11.15}$$

Note that this precoding matrix is a unitary matrix; that is, the precoding vector of the second stream is always chosen orthogonal to the one of the first stream. Although D-TxAA defines four precoding matrices, only the first two of them cause different SINRs at the receiver. In the other two cases, the SINRs of the first and the second stream are exchanged. Because the data rates of both streams can be adjusted individually, the third and fourth precoding matrices are redundant. Note also that if the user experiences low channel quality in D-TxAA, only a single stream is transmitted; that is, the precoding matrix in Equation (11.14) is applied to the data streams at the transmitter. Thus, in TxAA a single stream is always transmitted, and in D-TxAA either single-stream or double-stream transmission—whichever leads to a higher throughput—is performed. Details about the feedback calculation are provided in the next section.

11.2.4 Feedback Calculation

In MIMO HSDPA, two feedback values, the CQI and the precoding control indicator (PCI), must be calculated by the user equipment (UE) and fed back to the base station. In contrast to the receive power maximization suggested in [1], we perform a throughput-maximizing joint calculation of the CQI and the PCI [8]. This method has the advantage that it inherently provides a decision as to whether single-stream or double-stream transmission should be used.

The feedback calculation starts with the estimation of the post equalization SINR for *every* possible PCI value for single-stream and—where applicable—dual-stream transmission. All SINR values are reduced by a 1-dB margin (to account for SINR estimation errors) and then mapped to CQI values using Table 11.1 and Table 11.2 for single-stream and double-stream mode, respectively. The SINR-to-CQI mapping tables were obtained by simulating the block error ratio (BLER) performance of a category 16 UE

Table 11.1 SINR-CQI Mapping Table for Single-Stream Mode of a Category 16 UE

CQI	1	2	3	4	5	6	7	8
SINR	−3.5 dB	−2.6 dB	−1.5 dB	−0.3 dB	0.5 dB	1.7 dB	2.5 dB	3.5 dB
CQI	9	10	11	12	13	14	15	16
SINR	4.4 dB	5.5 dB	6.5 dB	7.5 dB	8.5 dB	9.5 dB	10.7 dB	11.5 dB
CQI	17	18	19	20	21	22	23	24
SINR	12.6 dB	13.4 dB	14.7 dB	15.7 dB	16.6 dB	17.5 dB	18.6 dB	19.6 dB
CQI	25	26	27	28	29	30		
SINR	20.6 dB	21.4 dB	22.6 dB	23.5 dB	24.0 dB	24.8 dB		

Table 11.2 SINR-CQI Mapping Table for Double-Stream Mode of a Category 16 UE

CQI	0	1	2	3	4	5	6	7
SINR	10.5 dB	10.5 dB	11.2 dB	12.7 dB	14.3 dB	15.7 dB	17.2 dB	18.8 dB
CQI	8	9	10	11	12	13	14	
SINR	20.4 dB	21.9 dB	23.4 dB	25.3 dB	26.0 dB	26.8 dB	28.3 dB	

for all CQI values in an additive white gaussian noise (AWGN) channel. The SINR values in the tables are equal to the AWGN signal-to-noise ratio (SNRs) at 10% BLER, as defined by the HSDPA standard [1, Section 6A.2] as the maximum BLER that should not be exceeded.

The CQI values obtained from the mapping tables correspond to transport block sizes (TBSs) defined in [1, Table 7D, p. 50] and [1, Table 7I, p. 54] for single-stream and double-stream mode, respectively. In double-stream mode, every PCI value yields two TBS values. Thus, by selecting the PCI value corresponding to the maximum overall TBS, the throughput is maximized. Note that this method inherently also provides the decision between single-stream and double-stream transmission.

In the case of Category 16 UE, the maximum TBS in single-stream mode is 25,558 bits that are transmitted in one sub-frame of length 2 ms. Thus, the maximum data rate in single-stream mode is 12.779 Mbps. In dual-stream mode, the maximum TBS of one stream is equal to 27,952 bits, allowing for a maximum overall data rate of 27.952 Mbps.

11.3 Measurement Setup and Procedure

In the following we report on our MIMO HSDPA measurement setup in an alpine and an urban scenario.[2] We furthermore explain in detail the measurement procedure utilizing our testbed [22,23].

11.3.1 Measurement Setup

Two scenarios were as follows:

- *Alpine scenario.* The base-station antenna (KATHREIN 800 10543 [24], ±45° polarization, half-power beam width 58°/6.2°, down tilt 6°) was placed 5.7 km away from the RX unit, which was located inside a

[2] For both measured scenarios, detailed transmitter and receiver positions can be downloaded for Google Earth at http://www.nt.tuwien.ac.at/fileadmin/data/testbed/Vienna-and-Carinthia-TX-RX-GPS.kmz.

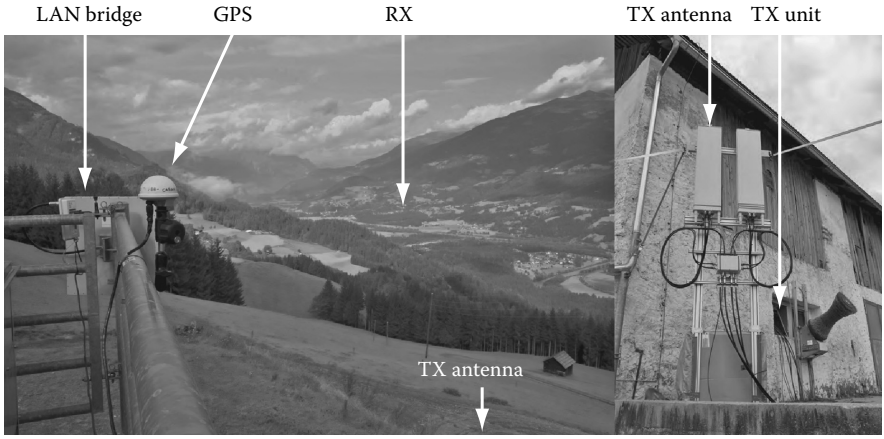

Figure 11.2 The alpine scenario and the base-station transmit antennas, of which the left one was utilized in the measurements.

house in a village on the opposite side of the "Drautal"-valley as shown in Figure 11.2. At the RX unit, we utilized standard Linksys WiFi-Router rod antennas. The results presented in the section "Measurement Results" were obtained in a setup in the alpine scenario in which the receive antennas were placed indoors in non-line-of-sight to the transmitter. This setup is characterized by a short mean RMS delay spread of about 1 chip (260 ns) and one major propagation path because the receive signal was mainly propagating through one window facing the transmit antennas. In addition to this setup, we also investigated RX antenna positions in different rooms where the TX antennas can and cannot be seen from the window. We also placed the RX unit outside, in the middle of a field, with direct line-of-sight to the transmitter. In all measured setups, the results obtained did not change significantly, apart from a variation in the average path loss that only shifts the throughput curves in Figure 11.6 to the left and right, respectively.

- *Urban Scenario.* The same base-station antenna (KATHREIN 800 10543 [24], ±45° polarization, half-power beam width 58°/6.2°, down tilt 6°) was placed on the roof of a big building in the center of Vienna, Austria, 430 m away from the RX unit that was placed inside an office room (see Figure 11.3). At the RX unit, we utilized four low-cost printed monopole antennas [25] that are based on the generalized Koch pre-fractal curve. Due to their low cost and small size, such antennas are very realistic and could be built into a mobile handset or a laptop computer. In all measurements carried out in the urban scenario, the direct path from the TX antennas to the RX antennas

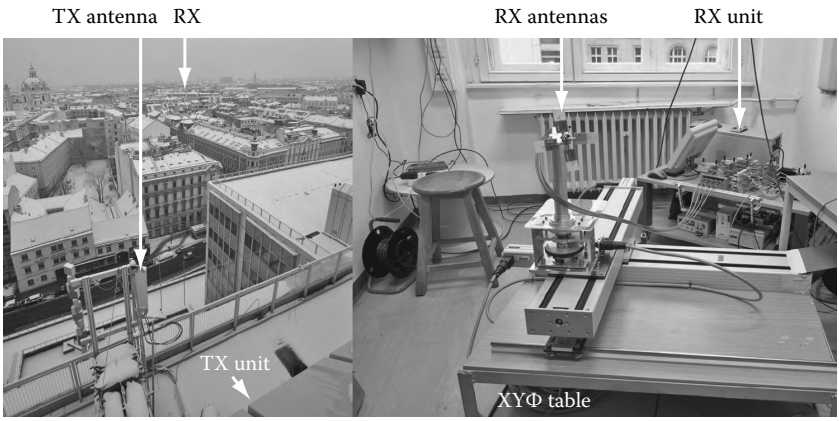

Figure 11.3 The urban scenario and the XYΦ positioning table with the receive antennas.

was blocked by the building in which the RX unit was located. This scenario is characterized by a rather long mean RMS delay spread of about 3.8 chips (1 μs).

In both scenarios, the transmit antennas were placed right next to existing base stations making the measurement results obtained very realistic and representative for a mobile communication system.

To exploit polarization diversity and to obtain good separation between the two spatial data streams, differently polarized antenna elements were employed at the transmitter and at the receiver.

Figure 11.4 shows the basic measurement setup used for all our measurements as well as the important system parameters. Prior to a measurement, the following steps were carried out (the numbers in the square brackets are typical values):

- The TX and RX units are set up and a control radio link (basically a wireless local area network (LAN) bridge) between the TX and RX units is established. [3 days]
- All required transmit-data-blocks are pre-generated in Matlab and then stored (in the form of 14-bit complex baseband data samples) on parallel solid-state hard disks to achieve an access time in the order of 1 ms. [2 hours]
- The rubidium+GPS stabilized "clocks" of the TX and RX units are reset to zero with a relative accuracy of ±20 ns. The handshaking required for this reset is carried out via the control radio link so that there is no need for a cable connection. To meet the accuracy required

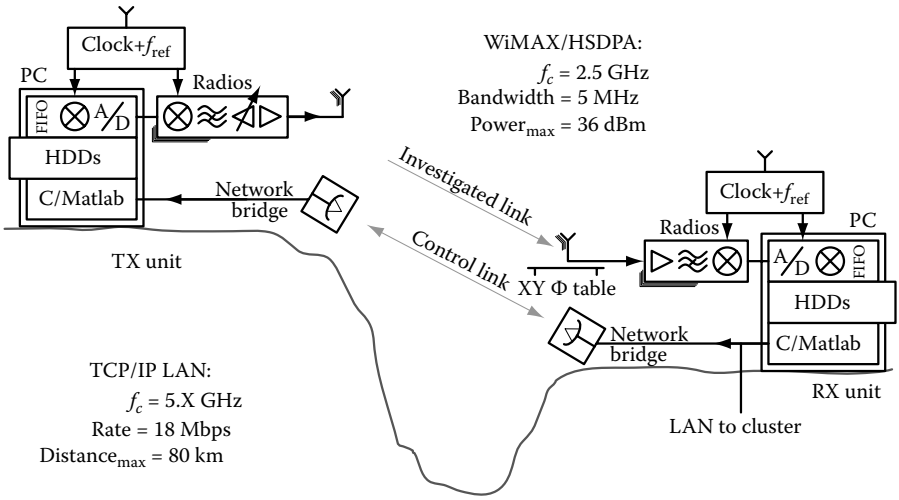

Figure 11.4 Measurement setup.

by typical measurements, this procedure takes less than half an hour from a cold start. The rubidium clocks also provide perfect frequency synchronization between transmitter and receiver. [30 min]

11.3.2 Measurement Procedure

Now we describe the transmission of an HSDPA block using our testbed (see also Figure 11.5). The required time for each operation is provided in square brackets at the end of each step.

- First, the RX unit (the master) requests the transmission of a "previous block" via the control link. (HSDPA requires the receiver to feed back information calculated from the previously received block in order to transmit a channel adapted signal.) [3 ms]

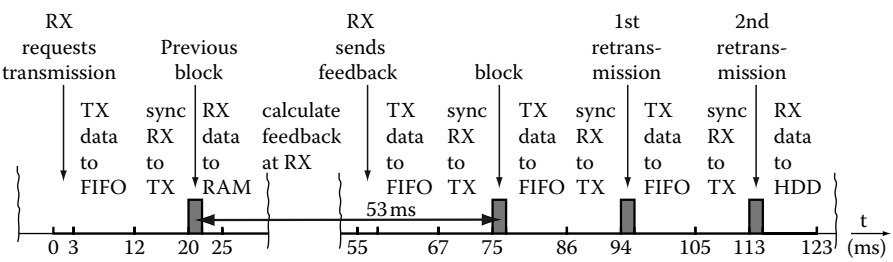

Figure 11.5 Timing of the transmission of a "single" data block.

- Then the transmitter copies the selected block (that is, pre-generated transmit data samples) from the solid-state hard disks to the FIFOs of the transmit hardware. [9 ms]
- Next, via the control link, the TX unit tells the RX unit the exact time that the transmission will take place—that is, current time plus 4 ms. (The delay of the control link is typically less than 4 ms.) Another 4 ms are required for the handshaking between PC and external synchronization hardware. [8 ms]
- Consequently, at exactly the same time, the transmission and the reception of a data block are triggered by the TX and the RX hardware, respectively.
- In real-time, the complex valued transmit data samples are interpolated to 200 MSamples/s, digitally up-converted to 70 MHz, converted to the analog domain (14 bit), analog up-converted to 2.5 GHz, attenuated (digitally adjustable), amplified, and then transmitted. At the receiver, exactly the reverse procedure takes place. At the end, the already down-sampled received complex baseband data samples are stored in the internal memory of the RX unit (not on the hard disks). [5 ms]
- These received samples are now immediately evaluated by the CPU of the RX computer, that is, synchronization, channel estimation, and feedback calculation are carried out in Matlab [8]. No further receiver processing is performed at this point. [$N_R \times 26$ ms]
- Now the RX unit requests the transmission of the actual channel-adapted data block via the control link (its index is determined by the feedback information calculated from the previous data block). Because we want to investigate the HSDPA performance when Hybrid Automated Repeat Request (HARQ) retransmissions are employed, the RX unit also requests the transmission of the two possible retransmissions, regardless of whether or not they are required. This is necessary because the data evaluation and determination of the required number of retransmissions are carried out later. [3 ms]
- Transmission of the three blocks now takes place in real-time (as described above). [57 ms]
- Finally, all four received blocks are stored on RAID hard disks for later/immediate off-line evaluation[3] in a cluster. [10 ms]

In our measurement, a typical value for the feedback delay between the "previous block" used for channel sounding and the actual transmission of the first channel-adapted data block is 53 ms, as shown in Figure 11.5. The

[3] We usually evaluate the first blocks of a measurement immediately in order to quickly discover possible flaws in the measurement setup (for example, power amplifiers still turned off or wrong buttons on the equipment pushed by accident).

actual time value depends on the MIMO HSDPA scheme under investigation. In a real HSDPA network, this feedback delay is on the order of a few milliseconds (at a maximum, 7.5 slots corresponding to 5 ms). Therefore, to obtain representative results, the measurement procedure requires the channel to stay constant during the feedback delay. Later off-line testing revealed that this is the case; that is, estimation of the feedback based on the "previous" blocks and the channel-adapted blocks did not show any significant difference. Note that the delays between the channel-adapted data block and the first and second retransmissions are about the same as in a real HSDPA network; thus, no further requirements on the measurement procedure are necessary.

11.3.3 Inferring the Average Performance

In the previous section, we explained in detail how a "single" HSDPA data block is transmitted. To infer the average throughput performance (as shown, for example, in Figure 11.6) of a specific scenario, we carry out the fully automatized following steps shown below:

- We repeat the procedure above for all different schemes under investigation (the curves in Figure 11.6).
- We repeat all the above for different transmit power levels (the x-axis in Figure 11.6). To achieve this, we attenuate the transmit signal prior to the power amplifier.
- We repeat all the above for different receive antenna positions (110 for the alpine scenario and 484 for the urban scenario). These realizations are created by moving the RX antennas with a fully automated XYΦ positioning table as shown in Figure 11.3. In order to minimize large scale fading effects, we measure only within a small area of 3×3 wavelengths. The measured antenna positions are uniformly distributed. By this systematic sampling approach, the distance between all positions measured is maximized and their correlations minimized.

Measuring all this typically takes from an hour up to a day. The evaluation of the data blocks (up to one terabyte of baseband data samples) is carried out using a self-programmed PC cluster software that parallelizes the off-line evaluation of the received data on a position-by-position basis on all currently available (typically about 20) employee PCs of our workgroup.

- Once calculated, we collect all results from the cluster in order to average the throughput observed over the positions measured. Several tests are carried out in order to validate the results; for example, we check for measurement outliers[4] or interference that should not exist.

[4] That does not mean that we discard them automatically. We check for their existence in order to detect possible flaws in the experiment setup.

- By measuring the output powers of all transmitters with a spectrum analyzer (Rohde and Schwarz FSQ26, relative accuracy ±0.1 dB), we ensured that our individual power adjustment done in the digital domain resulted in identical output powers. Nevertheless, we observed that the average receive powers originating from the individual transmit antennas differ by about 1 to 2 dB. To compensate for this effect when comparing HSDPA schemes with different numbers of transmit antennas, we therefore performed throughput averaging over the corresponding transmit/receive antennas. For example, if the 2 × 2 D-TxAA system is compared to the single input single output (SISO) transmission, the SISO throughput is obtained by averaging over the four individual SISO links (TX1→RX1, TX1→RX2, TX2→RX1, and TX2→RX2).
- Finally, we estimate the accuracy of the measurement by means of bootstrapping methods [26]. In all throughput graphs (Figures 11.6–11.7), the dots represent the average throughputs, the corresponding vertical lines the 95% confidence interval, and the corresponding horizontal lines the 2.5% and 97.5% percentiles. Note that the RX antenna positions remained unchanged between measuring different schemes at different transmit power levels. This, on one hand, leads to smooth curves. On the other hand, the *relative* positions of the curves are more accurate than the confidence intervals for the *absolute* positions might suggest.

11.4 Achievable Mutual Information

This section defines a so-called "achievable mutual information," which is used as a performance bound for the actually measured data throughput. The calculation of the bound is based on the mutual information between the transmit and the receive signals, that is, the estimated frequency response. The achievable data throughput is a function of the wireless channel and the allowed precoding vectors. Thus, it incorporates the restrictions given by the transmission standard (quantized, frequency-flat precoding) but not the restrictions given by the receiver employed.

Consider the time-dispersive channel of length L_b chips between the n_t-th transmit and the n_r-th receive antenna:

$$\mathbf{h}^{(n_r,n_t)} = \left[h_0^{(n_r,n_t)} \ \ldots \ h_{L_b-1}^{(n_r,n_t)} \right]^T \tag{11.16}$$

This channel can be equivalently described in the frequency domain as $\mathbf{g}^{(n_r,n_t)} = \mathcal{F}\mathfrak{F}\{\mathbf{h}^{(n_r,n_t)}\}$ using the N_{FFT} point Fourier transform $\mathfrak{F}\{.\}$. Thus, the Fourier transform separates the frequency-selective channel into N_{FFT}

frequency flat channels. The MIMO channel matrix of the m-th frequency bin can then be written as:

$$\mathbf{G}_m = \begin{bmatrix} \left(\mathbf{g}^{(1,1)}\right)_m & \cdots & \left(\mathbf{g}^{(1,N_T)}\right)_m \\ \vdots & \ddots & \vdots \\ \left(\mathbf{g}^{(N_R,1)}\right)_m & \cdots & \left(\mathbf{g}^{(N_R,N_T)}\right)_m \end{bmatrix}; \quad m = 1, \ldots, N_{\text{FFT}} \tag{11.17}$$

Using the well-known expressions for the MIMO capacity (see, for example, [27,28]), we obtain the achievable mutual information:

$$D_{\text{achievable}} = \max_{\mathbf{W}\in\mathcal{W}} \sum_{m=1}^{N_{\text{FFT}}} \frac{f_s}{N_{\text{FFT}}} \log_2 \det\left(\mathbf{I}_{N_R} + \frac{1}{\sigma_v^2}\mathbf{G}_m\mathbf{W}\mathbf{W}^H\mathbf{G}_m^H\right) \tag{11.18}$$

Here, f_s corresponds to the chip rate of HSDPA (3.84 MHz) and σ_v^2 to the variance of the noise $\mathbf{v}_k$. The maximization is performed over the set of all possible precoding matrices is $\mathcal{W}$. Note that Equation (11.18) represents neither the mutual information nor the channel capacity, because only quantized and frequency flat precoding is utilized in HSDPA. Therefore, $D_{\text{achievable}}$ is referred to as "achievable mutual information." Also note that Equation (11.18) only gives the achievable mutual information for a specific channel realization at a specific receive antenna position and a given transmit power level. To obtain a mean achievable mutual information, we perform averaging over all measured receive antenna positions. Also, because the channel is not known perfectly, we use the estimated channel coefficients at the largest transmit power (thus having the smallest possible channel estimation error) to calculate the achievable mutual information. At lower transmit powers, the different channel SNRs are obtained by scaling the channel coefficients accordingly.

11.5 Measurement Results

In this section we present the throughput measurement results (the solid lines in Figures 11.6 and 11.7) and compare them to the achievable mutual information (the dashed lines in Figures 11.6 and 11.7). All throughput curves are plotted versus transmit power. Two additional axes show the average received SISO SNR and average received SISO signal power. The reason we plot the throughput versus transmit power is the following: All MIMO schemes in HSDPA utilize adaptive precoding at the transmitter that effectively increases the received power and thus also the SNR, while the total transmit power is the same as in the SISO transmission. If the throughput is plotted versus SNR rather than versus transmit power, the curves will be shifted with respect to each other. For example, in case of TxAA, this

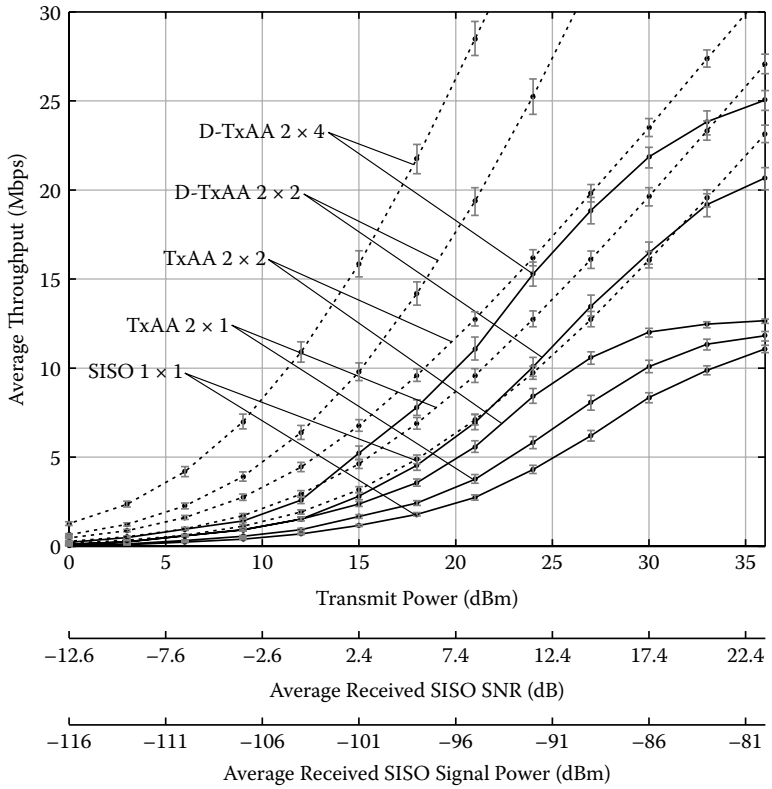

Figure 11.6 Throughput results of a category 16 UE in the alpine scenario (measurement ID "2008-09-16"). Averaging was performed over 110 receiver positions. The solid lines represent the measured throughput, the dashed lines the achievable mutual information.

shift would be about 2 dB compared to SISO. The additional *x*-axes (average received SISO SNR and average received SISO signal power) are thus only shown for reference reasons to indicate the approximate SNR and receive power ranges.

11.5.1 Alpine Scenario

Figure 11.6 shows the measured throughput and the achievable mutual information of the 1 × 1 SISO, 2 × 1 TxAA, 2 × 2 TxAA, 2 × 2 D-TxAA, and 2 × 4 D-TxAA transmission systems in the alpine scenario. Although all these schemes are standardized, only the 1 × 1 SISO transmission is currently (2009) implemented in HSDPA networks.

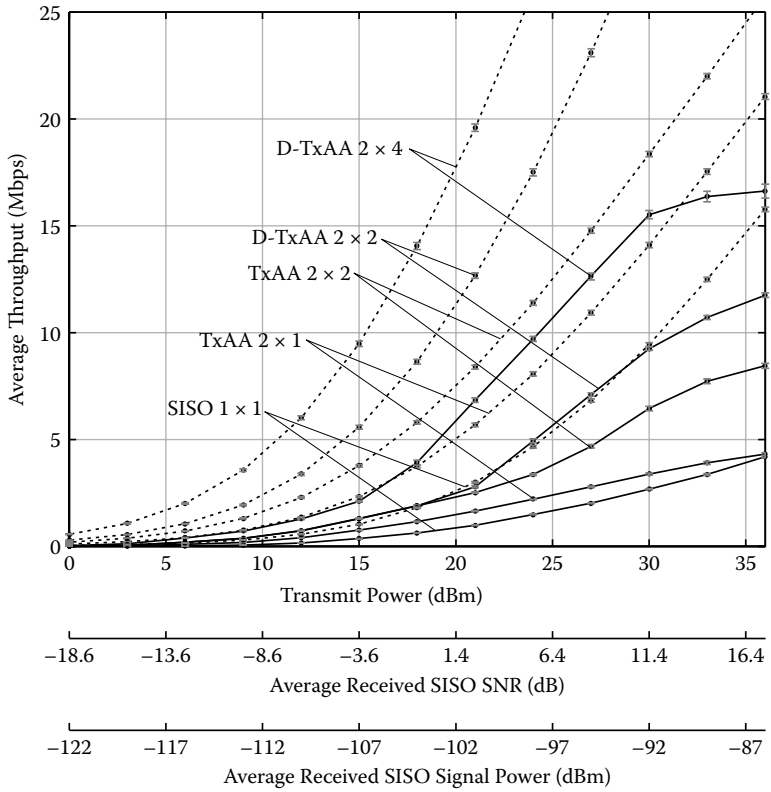

Figure 11.7 Throughput results of a category 16 UE in the urban scenario (measurement ID "2008-12-12"). Averaging was performed over 484 receiver positions. The solid lines represent the measured throughput, the dashed lines the achievable mutual information.

Figure 11.6 shows that the measured throughput of the 2 × 1 TxAA system is significantly (about 3 dB) better than the throughput of the SISO system. The 2 × 2 TxAA system performs another 3 dB better than the 2 × 1 TxAA system. The very good performance of the TxAA system in this scenario is explained by the rather small delay spread of the channel in which the frequency-flat precoding works very well. The 2 × 2 D-TxAA system performs better than the 2 × 2 TxAA system above transmit powers of 15 dBm. At certain receive antenna positions, D-TxAA thus employs double-stream transmissions outperforming the pure single-stream transmissions of TxAA. At all other receive antenna positions, D-TxAA switches back to single-stream operation. Compared to 2 × 2 D-TxAA, the 2 × 4 D-TxAA system achieves about 4 dB gain due to the doubled number of receive antennas.

The measured and the achievable mutual informations are compared at a transmit power of about 10 to 25 dBm or a throughput of about 5 Mbps to avoid saturation effects of the measured throughput (because outside this range either no more smaller or larger CQI values are available). At large transmit powers, when the single-stream transmission modes saturate, such a comparison would be misleading because the throughput could be easily increased by providing additional modulation and coding schemes (as it is done, for example, in UE categories 13, 14, 17, and 18 that support 64-QAM modulation [1]). At a throughput of 5 Mbps, the measured SISO system loses about 7 dB and the 2 × 2 D-TxAA system about 5 dB compared to their corresponding achievable mutual informations.

11.5.2 Urban Scenario

In Figure 11.7, the results of the standard compliant schemes in the urban scenario are shown. Here, at low SNR the 2 × 1 TxAA system only performs a little bit better than the SISO system and achieves only the same performance as SISO at large SNR. The reason for this is the rather large mean RMS delay spread of 3.8 chips (1 μs) causing the precoding to be far from optimal. Optimal precoding must be frequency dependent, for example, using a water-filling solution. The large delay spread also causes inter-code interference that can only be partially removed by the LMMSE equalizer, leading to a saturation of the throughput at larger transmit powers and SNRs. When using two or four receive antennas, the interference situation gets better because the equalizer can suppress the post-equalization interference more effectively. Thus, the two and four receive antenna schemes show greatly increased throughput in the urban scenario.

Due to the increased interference in the urban scenario, the loss between measured throughput and the achievable mutual informations is larger than in the alpine scenario. With increasing order of the MIMO system, the loss to the achievable mutual information decreases.

11.5.3 Discussion of the Throughput Loss

Although the results of the previous sections show a significant performance increase of the different MIMO schemes when compared to SISO transmission, all measured throughput curves are about 6 to 9 dB away from the achievable mutual information. The following effects contribute (next to maybe others) to this loss:

- The rate-matched Turbo code utilized in HSDPA is good but not optimal. AWGN simulations show that at higher code rates, it loses up to 2 dB when decoded by a MAP decoder. [approx. 2 dB]

- The LMMSE equalizer representing a low-complexity and cost-effective solution is also not optimal. Better receivers such as the LMMSE-MAP have the potential to improve the performance by about 1 dB [21]. [approx. 1 dB]
- In the urban scenario, a larger throughput loss than in the alpine scenario was measured because of the larger delay spread and, consequently, the larger inter-code interference. For example, in the alpine scenario, the SISO system loses about 7 dB to the achievable mutual information, whereas the loss in the urban scenario is about 9 dB [>2 dB in the urban scenario].

11.6 Summary

The physical layer MIMO HSDPA throughput measurement results shown in this chapter were obtained in two extensive measurement campaigns carried out in an alpine valley in Austria and in the inner city of Vienna, Austria. These scenarios differ significantly in the delay spread of the channel and consequently in the resulting intra-cell interference. In both scenarios, the use of multiple antennas considerably increases the physical layer throughput. The 2 × 2 D-TxAA system increases the physical layer throughput by more than a factor of two compared to the SISO system. Absolute values of the mean measured throughput at transmit powers of 20 and 30 dBm are summarized in Table 11.3.

As a performance bound for the measured throughput, the so-called "achievable" mutual information is defined. Its calculation is based on mutual information of the channel that includes the quantized precoding employed at the transmitter. Comparing the measured throughputs to their corresponding achievable matual informations shows that the measured

Table 11.3 Mean Measured HSDPA Throughput in the Alpine and Urban Scenarios at Transmit Powers $P_{TX} = 20$ dBm and $P_{TX} = 30$ dBm

	Alpine Scenario *260 ns Mean RMS Delay Spread*		*Urban Scenario* *1 μs Mean RMS Delay Spread*	
	$P_{TX} = 20$ dBm	$P_{TX} = 30$ dBm	$P_{TX} = 20$ dBm	$P_{TX} = 30$ dBm
1 × 1 SISO	2.4 Mbps	8.3 Mbps	0.9 Mbps	2.7 Mbps
2 × 1 TxAA	3.3 Mbps	10.1 Mbps	1.0 Mbps	2.8 Mbps
2 × 2 TxAA	4.9 Mbps	12.0 Mbps	1.7 Mbps	4.7 Mbps
2 × 2 D-TxAA	6.1 Mbps	16.5 Mbps	1.7 Mbps	7.1 Mbps
2 × 4 D-TxAA	10.0 Mbps	21.9 Mbps	3.3 Mbps	12.6 Mbps

throughput is far from optimal, losing between 5 and 9 dB in SNR, depending on the MIMO scheme employed. The main reasons for this are found to be coding loss, and equalizer loss, as well as losses due to residual intercode interference. Thus, a large potential for future optimizations exists.

11.7 Acknowledgments

This work has been funded by the Christian Doppler Laboratory for Wireless Technologies for Sustainable Mobility. The authors thank Constantine Kakoyiannis (National Technical University of Athens, Greece) for providing us with the printed monopole RX antennas utilized in our measurements. The TX antennas were provided by KATHREIN-Werke KG. Also, the authors thank José Antonio García Naya, Michal Šimko, Walter Schüttengruber, and Georg Maier for supporting us with setting up the testbed.

References

[1] 3GPP, Technical specification group radio access network; physical layer procedures (FDD) (Tech. Spec. 25.214 V7.7.0), November 2007. [Online]. Available: http://www.3gpp.org/ftp/Specs/html-info/25214.htm

[2] M. Nakamura, Y. Awad, and S. Vadgama, Adaptive control of link adaptation for high speed downlink packet access (HSDPA) in W-CDMA, in *Proc. 5th Int. Symp. on Wireless Personal Multimedia Commun. 2002*, 2: 382–386, October 2002. [Online]. Available: http://ieeexplore.ieee.org/stamp/stamp.jsp?arnumber=1088198

[3] A. Das, F. Khan, A. Sampath, and H.-J. Su, Performance of hybrid ARQ for high speed downlink packet access in UMTS, in *Proc. 54th IEEE Vehicular Technol. Conf. 2001 (VTC2001-Fall)*, 4: 2133–2137, 2001. [Online]. Available: http://ieeexplore.ieee.org/stamp/stamp.jsp?arnumber=957121

[4] H. Chao, Z. Liang, Y. Wang, and L. Gui, A dynamic resource allocation method for HSDPA in WCDMA system, in *Proc. 5th IEE Int. Conf. 3G Mobile Commun. Technol. 2004 (3G 2004)*, 2004, pp. 569–573. [Online]. Available: http://ieeexplore.ieee.org/stamp/stamp.jsp?tp=&arnumber=1434541

[5] R. Naja, J.-P. Claude, and S. Tohme, Adaptive multi-user fair packet scheduling in HSDPA network, in *Proc. Int. Conf. Innovations in Information Technol. 2008 (IIT 2008)*, December 2008, pp. 406–410. [Online]. Available: http://ieeexplore.ieee.org/stamp/stamp.jsp?tp=&arnumber=4781652

[6] R. Kwan, M. Aydin, C. Leung, and J. Zhang, Multiuser scheduling in HSDPA using simulated annealing, in *Proc. Int. Wireless Commun. Mobile Computing Conf. 2008 (IWCMC 2008)*, August 2008, pp. 236–241. [Online]. Available: http://ieeexplore.ieee.org/stamp/stamp.jsp?tp=&arnumber=4599941

[7] C. Mehlführer and M. Rupp, Novel tap-wise LMMSE channel estimation for MIMO W-CDMA, in *Proc. 51st IEEE Global Telecommun. Conf. 2008*

(GLOBECOM 2008), New Orleans, LA, November 2008. [Online]. Available: http://publik.tuwien.ac.at/files/PubDat_169129.pdf

[8] C. Mehlführer, S. Caban, M. Wrulich, and M. Rupp, Joint throughput optimized CQI and precoding weight calculation for MIMO HSDPA, in *Conf. Record 42nd Asilomar Conf. Signals, Systems and Computers*, Pacific Grove, CA, October 2008, pp. 1320–1325. [Online]. Available: http://publik.tuwien.ac.at/files/PubDat_167015.pdf

[9] M. Harteneck, M. Boloorian, S. Georgoulis, and R. Tanner, Practical aspects of an HSDPA 14 Mbps terminal, in *Conf. Record 38th Asilomar Conf. Signals, Systems and Computers, 2004*, Pacific Grove, CA, 1: 799–803, November 2004. [Online]. Available: http://ieeexplore.ieee.org/stamp/stamp.jsp?arnumber=1399246

[10] M. Harteneck, M. Boloorian, S. Georgoulis, and R. Tanner, Throughput measurements of HSDPA 14 Mbit/s terminal, *Electronics Lett.*, 41(7): 425–427, March 2005. [Online]. Available: http://ieeexplore.ieee.org/stamp/stamp.jsp?arnumber=1421242

[11] C. Mehlführer, S. Caban, and M. Rupp, Measurement based evaluation of low complexity receivers for D-TxAA HSDPA, in *Proc. 16th Eur. Signal Processing Conf. (EUSIPCO 2008)*, Lausanne, Switzerland, August 2008. [Online]. Available: http://publik.tuwien.ac.at/files/PubDat_166132.pdf

[12] M. Wrulich, C. Mehlführer, and M. Rupp, Interference aware MMSE equalization for MIMO TxAA, in *Proc. 3rd Int. Symp. Communications, Control and Signal Processing (ISCCSP 2008)*, St. Julians, Malta, March 2008, pp. 1585–1589. [Online]. Available: http://publik.tuwien.ac.at/files/pub-et_13657.pdf

[13] C. Mehlführer, M. Wrulich, and M. Rupp, Intra-cell interference aware equalization for TxAA HSDPA, in *Proc. 3rd IEEE Int. Symp. Wireless Pervasive Computing (ISWPC 2008)*, Santorini, Greece, May 2008, pp. 406–409. [Online]. Available: http://publik.tuwien.ac.at/files/pub-et_13749.pdf

[14] S. Geirhofer, C. Mehlführer, and M. Rupp, Design and real-time measurement of HSDPA equalizers, in *Proc. 6th IEEE Workshop on Signal Processing Advances in Wireless Communications (SPAWC 2005)*, New York City, June 2005, pp. 166–170. [Online]. Available: http://publik.tuwien.ac.at/files/pub-et_9722.pdf

[15] L. Mailaender, Linear MIMO equalization for CDMA downlink signals with code reuse, *IEEE Trans. on Wireless Commun.*, 4(5): 2423–2434, September 2005. [Online]. Available: http://ieeexplore.ieee.org/iel5/7693/32683/01532226.pdf

[16] R. Love, K. Stewart, R. Bachu, and A. Ghosh, MMSE equalization for UMTS HSDPA, in *Proc. 58th IEEE Vehicular Technol. Conf. 2003 (VTC2003—Fall)*, 4: 2416–2420, October 2003. [Online]. Available: http://ieeexplore.ieee.org/stamp/stamp.jsp?arnumber=1285963

[17] Y. Guo, J. Zhang, D. McCain, and J. Cavallaro, Efficient MIMO equalization for downlink multi-code CDMA: Complexity optimization and comparative study, in *Proc. 47th IEEE Global Telecommun. Conf. 2004 (GLOBECOM 2004)*, 4: 2513–2519, November 2004. [Online]. Available: http://ieeexplore.ieee.org/stamp/stamp.jsp?arnumber=1378459

[18] Y. Guo, J. Zhang, D. McCain, and J. R. Cavallaro, An efficient circulant MIMO equalizer for CDMA downlink: Algorithm and VLSI architecture, *EURASIP Journal on Applied Signal Processing*, Vol. 2006, Article ID 57134, 2006. [Online]. Available: http://www.hindawi.com/GetPDF.aspx?doi=10.1155/ASP/2006/57134

[19] G.H. Golub and C.F. van Loan, Eds., *Matrix Computations*, 3rd ed. The Johns Hopkins University Press, 1996.

[20] D. Garrett, G. Woodward, L. Davis, G. Knagge, and C. Nicol, A 28.8 Mb/s 4x4 MIMO 3G high-speed downlink packet access receiver with normalized least mean square equalization, in *Digest of Technical Papers IEEE Int. Solid-State Circuits Conf. 2004 (ISSCC 2004)*, 1: 420–536, February 2004. [Online]. Available: http://ieeexplore.ieee.org/stamp/stamp.jsp?arnumber=1332773

[21] J. Ylioinas, K. Hooli, K. Kiiskila, and M. Juntti, Interference suppression in MIMO HSDPA communication, in *Proc. 6th Nordic Signal Processing Symp. 2004 (NORSIG 2004)*, 2004, pp. 228–231. [Online]. Available: http://ieeexplore.ieee.org/stamp/stamp.jsp?arnumber=1344565

[22] S. Caban, C. Mehlführer, G. Lechner, and M. Rupp, Testbedding MIMO HSDPA and WiMAX, in *Proc. 70th IEEE Vehicular Technol. Conf. (VTC2009—Fall)*, Anchorage, AK, September 2009. [Online]. Available: http://publik.tuwien.ac.at/files/PubDat_176574.pdf

[23] S. Caban, C. Mehlführer, R. Langwieser, A. L. Scholtz, and M. Rupp, Vienna MIMO testbed, *EURASIP J. Appl. Signal Processing, Special Issue on Implementation Aspects and Testbeds for MIMO Systems*, Vol. 2006, Article ID 54868, 2006. [Online]. Available: http://publik.tuwien.ac.at/files/pub-et_10929.pdf

[24] Kathrein, Technical Specification Kathrein Antenna Type No. 800 10543. [Online]. Available: http://www.kathrein.de/de/mcs/produkte/download/9363438.pdf

[25] C. Kakoyiannis, S. Troubouki, and P. Constantinou, Design and implementation of printed multi-element antennas on wireless sensor nodes, in *Proc. 3rd Int. Symp. Wireless Pervasive Computing 2008 (ISWPC 2008)*, Santorini, Greece, May 2008, pp. 224–228. [Online]. Available: http://ieeexplore.ieee.org/stamp/stamp.jsp?arnumber=4556202

[26] B. Efron and D.V. Hinkley, *An Introduction to the Bootstrap (CRC Monographs on Statistics & Applied Probability 57)*, 1st ed. Chapman & Hall, 1994.

[27] I.E. Telatar, Capacity of multi-antenna Gaussian channels, Eur. Trans. Telecommun. 1999, Technical Memorandum, Bell Laboratories, Lucent Technologies, 10(6): 585–595, October 1998. [Online]. Available: http://mars.bell-labs.com/papers/proof/proof.pdf

[28] G.J. Foschini and M.J. Gans, On limits of wireless communication in a fading environment when using multiple antennas, *Wireless Personal Commun*. 6(3): 311–335, 1998. [Online]. Available: http://www.springerlink.com/content/h1n7866218781520/fulltext.pdf